Research Article Vol. 39, No. 9 / September 2022 / Journal of the Optical Society of America B 2395

Journal of the Optical Society of America B

OPTICAL PHYSICS

Radially polarized 33 W emission from a double-pass Ho:YAG thin-slab amplifier

MATTHEW J. BARBER,* PETER C. SHARDLOW, CALLUM R. SMITH, AND W. ANDREW CLARKSON

Optoelectronics Research Centre, University of Southampton, Southampton, SO17 1BJ, UK
**Corresponding author: m.j.barber@soton.ac.uk*

Received 2 June 2022; revised 23 July 2022; accepted 23 July 2022; posted 25 July 2022; published 11 August 2022

The generation of a 33.7 W radially polarized output is demonstrated by way of double-pass amplification in a Ho:YAG thin-slab crystal. The amplifier system was seeded with the radially polarized output beam from a continuous-wave 13.2 W, 2.1 μm Ho:YAG rod laser, which exploited gain medium bifocusing and a ring-shaped pump spot to promote preferential lasing on the radially polarized Laguerre–Gaussian mode. By compensating for both the thermally induced stress birefringence in the thin-slab crystal and the Gouy phase shift resulting from astigmatic focusing of the 13.2 W seed, only marginal beam degradation was observed across the 95 W range of pump power into the amplifier.

Published by Optica Publishing Group under the terms of the Creative Commons Attribution 4.0 License. Further distribution of this work must maintain attribution to the author(s) and the published article's title, journal citation, and DOI.
https://doi.org/10.1364/JOSAB.465778

1. INTRODUCTION

Radially polarized laser beams are characterized by a donut-shaped intensity profile, where the polarization direction at each point in the beam is orientated in the radial direction. As a result of these unique properties, radially polarized beams have found applications in a range of areas including particle acceleration, particle trapping, and laser processing of materials [1–3]. In laser cutting applications, the action of the laser is to provide localized heating on a rapid timescale in order to achieve localized melting or vaporization. Therefore, efficient absorption of optical radiation by the material in question is fundamental to the laser cutting process. After piercing through a sheet material, the laser beam can be incident on the cutting front at a large angle of incidence, such that the reflectivity (and hence absorption) is strongly dependent on the polarization direction. In particular, the *p*-component of polarization (perpendicular to the plane of incidence) demonstrates a much lower reflectivity and hence a much higher absorption than the *s*-component of polarization. Therefore, in order to maximize the absorption of laser light, one would ideally like to use a laser beam where the polarization distribution is tailored to have each element of the beam striking each point on the cutting front with perfect *p*-polarization.

Radially polarized laser modes are particularly well-suited to achieve this configuration, as the polarization vectors are all directed away from the center of the beam profile [4]. For the cutting of sheet metals, radially polarized light may achieve a cutting efficiency that is up to 1.5–2 times higher than a linearly polarized or circularly polarized beam [5]. Not surprisingly, scaling the average power of radially polarized beams to meet the needs of laser cutting applications has been the subject of much interest, with recent studies investigating different amplifier architectures (such as thermally guiding fiber rods, single-crystal fibers, face-pumped thin disks and edge-pumped thin slabs [6–9]) in order to increase the power from a radially polarized master oscillator whilst preserving the beam quality and radial polarization purity.

In particular, the thin-slab geometry offers very favorable thermal management due to the two large contact faces, allowing near-one-dimensional heat transfer out of the gain medium. In addition, the thin-slab crystal can generally achieve a high level of gain extraction for efficient amplification without the need for a more complex multi-pass arrangement that is often utilized for thin-disk amplifiers. While the strong astigmatic focusing of a radially polarized beam into a thin slab results in a distorted polarization profile due to the different phase shifts experienced by the constituent Hermite–Gaussian (HG) modes—namely, HG_{01} and HG_{10}—this can often be corrected after amplification with a half-wave plate [9]. However, when the pump power is increased, stress-induced birefringence in the thin-slab crystal will produce an additional phase shift between the orthogonally polarized components, further degrading the radial polarization purity.

Here, we report on a modified design for a double-pass thin-slab amplifier, where the phase shift due to stress-induced birefringence and the Gouy phase shift are both corrected in order to produce a high quality radially polarized amplified beam. This scheme has been demonstrated for a double-pass

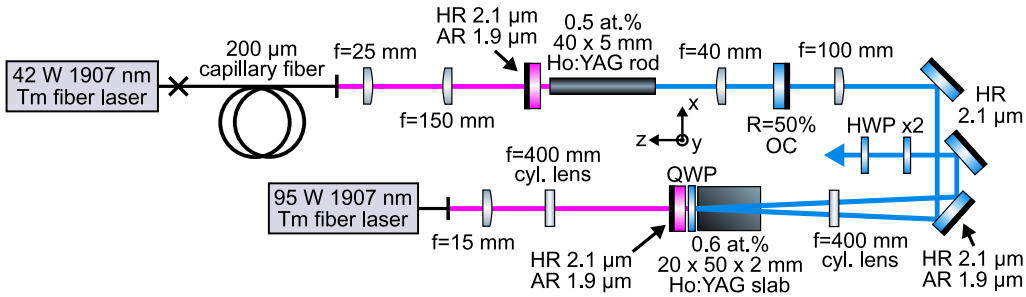

Fig. 1. Optical schematic of the radially polarized Ho:YAG rod seed laser and the double-pass Ho:YAG thin-slab amplifier.

Ho:YAG thin-slab amplifier at 2.1 μm, motivated by potential applications in the laser cutting of transparent polymers. The Ho:YAG amplifier was seeded by a 13.2 W radially polarized Ho:YAG rod master oscillator with a beam propagation factor (M^2) of 2.03 and a radial polarization purity of 10:1 and yielded an amplified output power of up to 33.7 W when pumped with 95 W of power from a single-mode 1907 nm thulium fiber laser. The amplified output beam had an M^2 value of 2.19 and a radial polarization purity of 8:1.

2. SEED LASER CONFIGURATION

The radially polarized Ho:YAG seed laser was constructed, as shown in Fig. 1, using a simple 245-mm-long two-mirror linear resonator design that was tailored to exploit thermally induced bifocusing as the means to achieving preferential lasing on the radially polarized Laguerre–Gaussian (LG_{01}) mode [10,11]. The resonator was formed between a plane-parallel input coupler mirror, which was highly reflective (HR) at 2.1 μm and anti-reflection (AR)-coated at 1.9 μm, and a plane-parallel output coupler (R = 50% at 2.1 μm, AR at 1.9 μm). The chosen Ho:YAG gain medium was a 40-mm-long, 5 mm diameter rod crystal with a 0.5 at.% Ho^{3+} doping concentration. The latter had AR coatings at 1.9 and 2.1 μm on both end faces and was mounted in a water-cooled copper heat-sink held at 20°C and positioned adjacent to the input coupler mirror. An intra-cavity $f = 40$ mm plano-convex lens was utilized in front of the output coupler mirror, such that careful variation of the lens–mirror distance could modify the cavity mode size and permit selection of the radially polarized LG_{01} mode.

Pump power was provided by a thulium-doped fiber laser with a maximum output power of 42 W at 1907 nm. The pump beam was conditioned by coupling it into the annular guide of a (ring-shaped) capillary fiber with a 200 μm outer diameter and a 100 μm diameter central hole. The output from the latter was relay imaged with the aid of a $f = 25$ mm collimating lens and a $f = 150$ mm focusing lens into the Ho:YAG crystal, producing a ring-shaped near-field pump beam profile with a 1.2 mm waist diameter in order to provide good spatial overlap with the LG_{01} mode within the Ho:YAG rod. Lastly, the radially polarized output beam was collimated by a $f = 100$ mm lens to produce a beam diameter of approximately 3.4 mm.

In operation, the Ho:YAG seed laser generated up to 13.2 W of output power, limited by the maximum available 1907 nm pump power, with a 19 W threshold and a 61% slope efficiency with respect to launched pump power (Fig. 2). The power curve

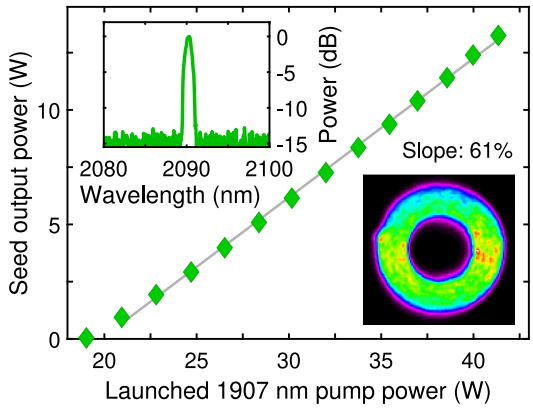

Fig. 2. Output power curve for the radially polarized Ho:YAG seed laser. Inset, top left: emission spectrum at 13.2 W. Inset, bottom right: near-field ring-shaped pump beam profile.

shows some slight deviation from a linear trend attributed to changes in the operating cavity mode with increasing pump power. In particular, the emission profile tends to have a larger fundamental LG_{00} mode content at lower pump powers, only becoming the radially polarized LG_{01} mode at around 40 W of incident pump. Selection of a radially polarized output exploits the small difference in thermal lens focal lengths for radially polarized and azimuthally polarized modes (i.e., bifocusing) in this cavity configuration, so there is a relatively small window of operation in terms of pump power to achieve a high quality radially polarized output beam.

Measurement of the laser emission spectrum was performed using a Yokogawa AQ6375B spectrum analyzer, indicating laser output only at 2090 nm. An image of the beam intensity profile was captured using a microbolometer camera (FLIR Lepton 3.0), demonstrating a ring-shaped laser output profile, which is consistent with the desired LG_{01} mode, as shown in Fig. 3(a). Additional images of the intensity profile were collected after passing the beam through a linear polarizer positioned in front of the imaging camera [Figs. 3(b)–3(e)]. The observation of a two-lobe profile, which is aligned with the linear polarizer axis in all four images, is strongly indicative of a radially polarized laser output. In order to quantify the radial polarization purity of the beam, the intensity variation along a circular path, which intersects both maxima of the two-lobe profile, was analyzed for each image [12]. As a result, the radial polarization purity is defined as the ratio between the maximum and minimum pixel intensity values along the circular path averaged over the

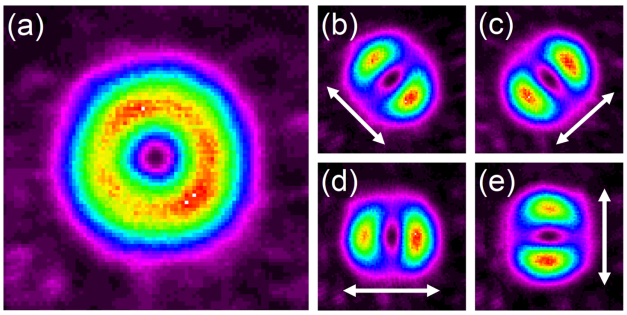

Fig. 3. (a) Beam intensity profile from the 13.2 W Ho:YAG seed laser. (b)–(e) Images of the seed beam after passing through a rotated linear polarizer, whose axis is shown by the arrows.

four different orientations of the linear polarizer, yielding a value for the radial polarization purity of more than 10:1. The beam propagation factor (M^2) of the seed laser source was measured at the maximum output power using an Ophir Nanoscan scanning-slit profiler, demonstrating an M^2 of 2.03 and 2.00 in the x and y directions, respectively. Such values are very close to the theoretical M^2 of 2.00 for a pure LG_{01} mode, confirming that the seed laser generated a high quality radially polarized LG_{01} output.

3. THIN-SLAB AMPLIFIER CONFIGURATION

Amplification of the 13.2 W seed laser output was performed in a 0.6 at.%-doped Ho:YAG thin-slab crystal, which had a 50 mm length (z dimension), 2 mm height (y), and 20 mm width (x). Both of the 20 mm by 2 mm end faces were AR-coated for 1.9 and 2.1 μm wavelengths. The crystal was mounted in a water-cooled copper heat-sink maintained at 20°C and designed to cool the large 50 mm by 20 mm faces, with 50-μm-thick indium foil serving as the thermal interface material.

The output beam from the seed laser was directed into the Ho:YAG thin slab using zero phase shift 45° mirrors to prevent degradation in radial polarization purity and was focused down in the $y-z$ plane using a $f=400$ mm cylindrical lens. The focused seed beam had dimensions of 3.4 mm ($x-z$ plane) and 660 μm ($y-z$ plane) at the waist, for which the Rayleigh range of the seed beam in the $y-z$ plane was calculated to be 150 mm. The seed light was injected at a small angle with respect to the long (z) axis of the thin slab to allow the amplified output beam to be extracted following a double pass. The system was configured such that the seed beam waist occurred around 12 mm behind the thin-slab crystal, where a flat dichroic mirror (HR at 2.1 μm, AR at 1.9 μm) was positioned parallel to the thin-slab input and output faces. Following the second pass through the Ho:YAG crystal, the amplified output beam was collimated by the same $f=400$ mm cylindrical lens.

At high power levels, thermally induced stress birefringence in the thin slab produces a small refractive index change that differs in the x and y directions, causing a phase shift between the constituent orthogonally polarized HG_{01} and HG_{10} modes after traversing the thin slab. The net result is a degradation in the radial polarization purity, which worsens with increasing pump power. In order to remedy this problem, a quarter-wave plate was inserted between the thin-slab crystal and the dichroic mirror, which was aligned with its fast (or slow) axis orientated at 45° to the x, y directions, so that the polarization directions of the two constituent HG_{01} and HG_{10} modes are rotated by 90° before making the second pass through the thin slab. As such, the phase shift due to thermally induced stress birefringence between the HG_{01} and HG_{10} modes acquired on the first pass through the thin slab is effectively cancelled out on the second pass. However, the quarter-wave plate introduces a net π phase shift between the HG_{01} and HG_{10} modes, in addition to a 90° rotation of their orthogonal polarization directions, which must be compensated to restore radial polarization.

There is however an additional phase shift produced between the HG_{01} and HG_{10} modes due to the strong astigmatic focusing of the seed beam that is required to inject it into the thin-slab crystal, known as the Gouy phase shift. The magnitude of Gouy phase accumulated by a particular HG mode can be expressed as

$$\phi_{\text{Gouy}} = (2n+1)\arctan\left(\frac{L}{z_{\text{R}x}}\right) + (2m+1)\arctan\left(\frac{L}{z_{\text{R}y}}\right), \tag{1}$$

where L is the total length of the astigmatic region, z_{R} is the Rayleigh range of the beam in the horizontal ($x-z$) or vertical ($y-z$) planes, and n, m are the indices of the HG_{nm} mode [13]. In the thin-slab amplifier configuration used here, L is equal to 800 mm, which is much shorter than the Rayleigh range of the unfocused horizontal seed beam dimension, causing the first term of Eq. (1) to tend towards zero. On the other hand, L is much larger than the 150 mm Rayleigh range of the tightly focused vertical dimension of the input seed beam, such that the second term of Eq. (1) tends towards $(2m+1)\pi/2$. As a result, it can be seen that the HG_{01} mode will develop a Gouy phase of $3\pi/2$, whilst the HG_{10} mode will develop a Gouy phase of $\pi/2$, with a net phase shift of π between the two modes. When taking into account the Gouy phase shift and the effect of the quarter-wave plate, the overall phase shift imparted on the constituent modes—combined with polarization rotations—results in an output beam with azimuthal polarization, despite a radially polarized beam initially being injected into the amplifier. However, the radial polarization can subsequently be restored by passing the amplified output through two half-wave plates orientated with a 45° angle between their fast axes, which acts as a 90° optical rotator.

The thin-slab amplifier crystal was counter-pumped by a 95 W, 1907 nm continuous-wave thulium fiber laser, which itself was free-space-pumped by a 240 W, 793 nm diode laser. The 1907 nm pump light was delivered via a passive fiber with a 10 μm core diameter, and residual (unabsorbed) 793 nm pump light was removed by a 45° dichroic mirror. An important parameter for efficient amplification is the spatial overlap between the incident seed light and the pump beam throughout the length of the amplifier crystal. Based on the ring-shaped profile of the LG_{01} mode, it may appear desirable to condition the amplifier pump beam into a ring geometry in order to maximize spatial overlap in a similar manner to the pump source of the seed laser.

However, due to the relatively small waist dimensions that must be achieved in the minor axis of the elliptical beam spot for pumping the thin slab, the use of a multimode capillary fiber for re-shaping the beam is inappropriate, as the resulting pump

beam would have a Rayleigh range that is much shorter than the length of the thin-slab crystal. Instead, the fundamental mode output from the 95 W thulium-doped fiber laser was used directly, sacrificing a certain level of beam shape similarity for more uniform pump intensity and more uniform excitation density in the amplifier crystal. As a majority of the fundamental mode pump beam intensity is in the center, it is beneficial for the pump beam to be sufficiently larger than the seed beam in the thin slab to ensure optimal spatial overlap between the seed beam intensity and the pumped region of the crystal.

The 1907 nm output beam from the thulium fiber laser was collimated using a $f = 15$ mm spherical lens and focused down in the $y - z$ plane using a $f = 400$ mm cylindrical lens to yield beam waist dimensions of 3.6 mm (horizontal) by 270 μm (vertical). In order to have the pump beam suitably larger than the seed at all times, the pump waist in the $y - z$ plane was formed 70 mm in front of the thin-slab crystal, such that the pump beam and seed beam would both be diverging during their propagation away from the amplifier mirror. In particular, beam simulations suggest that the minor diameter of the pump beam varies from 700 to 940 μm between the two end faces of the thin slab, while the minor diameter of the seed beam varies from 670 to 740 μm. The major (unfocused) diameters of the pump and seed remain at around 3.6 and 3.4 mm, respectively, throughout the thin-slab crystal. The elliptical seed beam area of around 1.9 mm^2 in the center of the thin-slab crystal produces a calculated saturation power, P_{sat}, of about 14 W, such that the system is operated close to the saturated regime ($P_{seed}/P_{sat} \approx 1$), where high efficiency amplification can be achieved.

For 13.2 W of radially polarized seed laser input, the thin-slab amplifier generated up to 33.7 W of output power, limited by the thulium fiber laser pump power (Fig. 4). The double-pass amplification had a 33% slope efficiency with respect to absorbed pump power and a 23% extraction efficiency, suggesting that the chosen seed beam dimensions have enabled a useful level of the thin-slab population inversion to be utilized. The variation in amplifier gain as a function of absorbed pump power is shown as an inset in Fig. 4, requiring 31 W of 1907 nm pump to reach transparency in the amplifier and reaching a maximum gain of 4 dB for an absorbed pump power of 89 W. An additional inset in Fig. 4 visualizes the simulated variation in seed and pump beam areas throughout the length of the thin-slab crystal, showing both beams diverging away from the amplifier mirror.

A key limitation to the efficiency of the Ho:YAG amplifier can be attributed to the imperfect spatial overlap between the seed and pump profiles, particularly around the central intensity minimum of the radially polarized beam, where almost none of the thin-slab population inversion can typically be extracted. An additional constraint on the system was the need to tilt the amplifier mirror away from normal incidence in order to reduce feedback instabilities in the 1907 nm pump laser and heating of the free-space diode coupling optics. As a result, the second pass of the seed light through the thin slab had poorer overlap with the region of population inversion than the first pass, producing a lower power extraction. Further improvement of the system could be achieved by striking a better balance between the pump beam area needed for a more accessible transparency power and the seed beam area needed for operating in the saturated

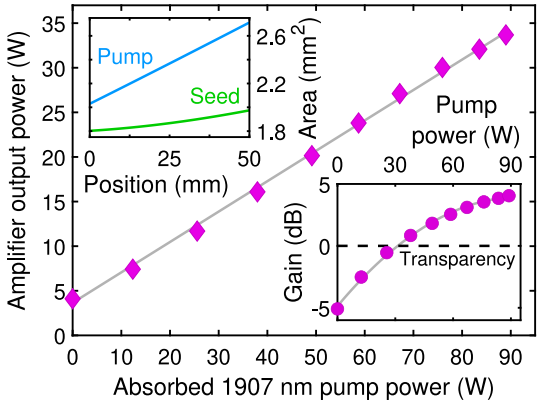

Fig. 4. Output power curve for the Ho:YAG thin-slab amplifier with a 13.2 W seed input. Inset, top left: simulated variation in pump and seed beam areas along the length of the crystal. Inset, bottom right: amplifier gain versus absorbed pump.

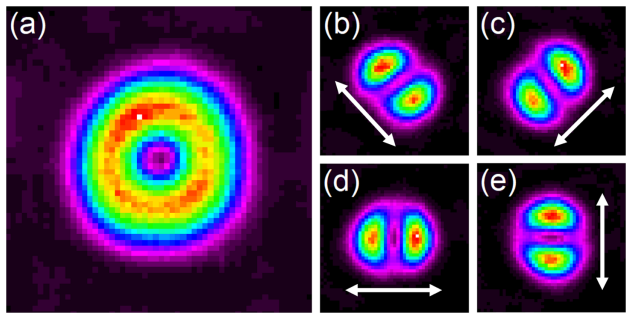

Fig. 5. (a) Beam intensity profile of the 33.7 W output from the Ho:YAG thin-slab amplifier. (b)–(e) Images of the beam passed through a rotated linear polarizer, with the transmission axis shown by the arrows.

regime. In addition, the use of a pump beam spot with a longer Rayleigh range should permit greater maintenance of the beam overlap throughout the crystal and enable a higher extraction efficiency to be achieved. On the other hand, to increase the gain of the amplifier, it could be beneficial to utilize a much higher power 1907 nm pump source and/or to use a greater dopant concentration and a longer crystal length (to improve the pump absorption efficiency).

At 33.7 W of output from the amplifier, the beam intensity profile shows a minor degradation in uniformity [Fig. 5(a)], but generally maintains the ring-shaped geometry of the LG_{01} mode. Measurement of the M^2 for the amplifier output indicated values of 2.19 and 2.16 in the horizontal and vertical directions, respectively, remaining relatively close to the performance of the seed source. Imaging of the beam through a linear polarizer suggested that the amplifier emission was still radially polarized due to the observation of a two-lobe intensity pattern, which was aligned with the polarizer's transmission axis at multiple orientations of the polarizer [Figs. 5(b)–5(e)]. Analysis of the radial polarization purity for the amplifier output beam was performed using the same procedure as that used for the seed laser, demonstrating a purity value of 8:1. The relatively small reduction in polarization purity indicates that the degrading effects of stress birefringence and Gouy phase shifts have

been successfully suppressed in the amplifier system. As a result, further power scaling of the thin-slab amplifier should be readily accessible with an improved (all-fiber) pump source and a higher power seed laser.

4. CONCLUSION

The power scaling of radially polarized laser emission is often impacted by the onset of beam degradation, which arises from thermally induced effects in the gain medium. Here, a 13.2 W radially polarized Ho:YAG rod laser has been demonstrated, utilizing an intra-cavity plano-convex lens and ring shaping of the pump beam in order to produce more favorable lasing conditions for the radially polarized LG_{01} mode than other transverse modes. A double-pass Ho:YAG thin-slab amplifier system been utilized to increase the radially polarized output power up to 33.7 W when edge-pumped from the opposite side with a 95 W, 1907 nm single-mode thulium fiber laser. The stress birefringence generated in the thin-slab crystal at high power levels has been compensated by rotating the polarization of the radially polarized beams constituent modes by 90° in between the first and second passes of the amplifier. Furthermore, the impact of the Gouy phase shift generated by strong astigmatic focusing was addressed, allowing a radially polarized beam to be maintained after double-pass amplification. At 33.7 W of output power, the beam emitted from the thin-slab amplifier demonstrated a maximum M^2 of 2.19 and a radial polarization purity value of 8:1, suggesting that only slight degradation of the radially polarized seed beam had been introduced during propagation through the amplifier system. Such performance highlights the Ho:YAG thin-slab amplifier as a very promising architecture for high average power 2.1 μm radially polarized beam generation to target a wealth of laser applications.

Funding. Engineering and Physical Sciences Research Council (EP/P027644/1).

Acknowledgment. M. J. B. acknowledges financial support from the EPSRC (2115206) and Leonardo UK.

Disclosures. The authors declare no conflicts of interest.

Data availability. The data underpinning this publication is available from the University of Southampton repository [14].

REFERENCES

1. M. Wen, Y. I. Salamin, and C. H. Keitel, "Electron acceleration by a radially-polarized laser pulse in a plasma micro-channel," Opt. Express **27**, 557–566 (2019).
2. Q. Zhan, "Trapping metallic Rayleigh particles with radial polarization," Opt. Express **12**, 3377–3382 (2004).
3. R. Weber, A. Michalowski, M. Abdou-Ahmed, V. Onuseit, V. Rominger, M. Kraus, and T. Graf, "Effects of radial and tangential polarization in laser material processing," Phys. Procedia **12**, 21–30 (2011).
4. A. V. Nesterov and V. G. Niziev, "Laser beams with axially symmetric polarization," J. Phys. D **33**, 1817–1822 (2000).
5. V. G. Niziev and A. V. Nesterov, "Influence of beam polarization on laser cutting efficiency," J. Phys. D **32**, 1455–1461 (1999).
6. T. L. Jefferson-Brain, C. R. Smith, M. D. Burns, P. C. Shardlow, and W. A. Clarkson, "Amplification of a radially polarized beam in a thermally guiding ytterbium-doped fiber rod," Appl. Phys. B **125**, 167 (2019).
7. F. Beirow, M. Eckerle, T. Graf, and M. A. Ahmed, "Amplification of radially polarized ultra-short pulsed radiation to average output powers exceeding 250 W in a compact single-stage Yb:YAG single-crystal fiber amplifier," Appl. Phys. B **126**, 148 (2020).
8. A. Loescher, J.-P. Negel, T. Graf, and M. Abdou Ahmed, "Radially polarized emission with 635 W of average power and 21 mJ of pulse energy generated by an ultrafast thin-disk multipass amplifier," Opt. Lett. **40**, 5758–5761 (2015).
9. C. R. Smith, S. J. Beecher, J. I. Mackenzie, and W. A. Clarkson, "Amplification of a radially polarised beam in an Yb:YAG thin-slab," Appl. Phys. B **123**, 225 (2017).
10. J. W. Kim, J. I. Mackenzie, J. R. Hayes, and W. A. Clarkson, "High power Er:YAG laser with radially-polarized Laguerre-Gaussian (LG_{01}) mode output," Opt. Express **19**, 14526–14531 (2011).
11. P. C. Shardlow, M. J. Barber, A. C. Butler, and W. A. Clarkson, "Hybrid Ho:YAG laser with 50 W radially-polarised output," in *Conference on Lasers and Electro-Optics Europe and European Quantum Electronics Conference* (2019), paper CA_1_2.
12. D. Lin, J. M. O. Daniel, M. Gecevičius, M. Beresna, P. G. Kazansky, and W. A. Clarkson, "Cladding-pumped ytterbium-doped fiber laser with radially polarized output," Opt. Lett. **39**, 5359–5361 (2014).
13. M. Beijersbergen, L. Allen, H. van der Veen, and J. Woerdman, "Astigmatic laser mode converters and transfer of orbital angular momentum," Opt. Commun. **96**, 123–132 (1993).
14. M. J. Barber, P. C. Shardlow, C. R. Smith, and W. A. Clarkson, "Dataset to support the paper '33 W radially polarized emission from a double-pass Ho:YAG thin-slab amplifier'," University of Southampton, 2022, https://doi.org/10.5258/SOTON/D2237.

152.78.211.177 (ip 2022-09-01 04:46:50)